Infrared reflectance of thick *p*-type porous SiC layers

M. F. MacMillan, R. P. Devaty,[a)] and W. J. Choyke
Department of Physics and Astronomy, University of Pittsburgh, Pittsburgh, Pennsylvania 15260

D. R. Goldstein, J. E. Spanier, and A. D. Kurtz
Kulite Semiconductor Products, Inc., One Willow Tree Road, Leonia, New Jersey 07605

Thick *p*-type porous 6H SiC layers were fabricated by anodization of *p*-type 6H SiC bulk crystals in dilute HF. Striking differences are observed in the reststrahl region room-temperature reflectance of these porous layers compared to that of bulk 6H SiC crystals. Instead of the single broad band reflectance spectrum typically observed in bulk 6H SiC, a two-band reflectance spectrum is observed. Several effective medium models, based on different morphologies of the component materials, 6H SiC and air, are used to obtain the frequency-dependent dielectric function of porous SiC from which calculated reflectance spectra are generated. The best match between measured and calculated spectra is obtained for a Maxwell–Garnett model with SiC acting as the host material and air cavities acting as the inclusion material. The model reproduces the two reflectance band structure observed in the measured reflectance of the porous SiC layers. The differences in the reststrahl region reflectance spectra of the porous SiC layers, compared to bulk SiC, are associated with polarization effects introduced by the cavities combined with a mean field average of interactions among the cavities. © *1996 American Institute of Physics.* [S0021-8979(96)03716-4]

I. INTRODUCTION

Recently there has been much interest in the development of porous semiconductor materials which have potential applications for optoelectronic devices. The most studied of these materials is porous silicon, which exhibits bright photoluminescence above the Si band gap (1.1 eV).[1] Porous gallium phosphide[2] and silicon germanium[3] have also been reported. Both *n*-type[4–7] and *p*-type[8] porous 6H SiC have been fabricated. *p*-type porous SiC has been studied primarily with transmission electron microscopy,[8,9] cathodoluminescence,[8,9] and photoluminescence.[10]

In this article we present room-temperature infrared reflectance measurements of thick, monocrystalline, *p*-type porous 6H SiC layers. These samples were fabricated by anodization of *p*-type 6H–SiC bulk crystals in dilute HF. Striking differences can be seen in the reststrahl region reflectance of these porous layers compared to that of bulk 6H SiC crystals. Similar behavior was recently reported for *n*-type porous 6H SiC.[7] Effective medium theories are often used to interpret the optical properties of microscopically imhomogeneous media in terms of their composition and microstructural morphology.[11] Several effective medium models based on different morphologies of the component materials were used to model the frequency-dependent dielectric function of porous SiC. These models include two versions of the Maxwell–Garnett model,[12] the Bruggeman model,[13] and a simplified version of a model introduced by Sheng.[14,15] Calculated reflectance spectra generated using these dielectric functions are compared to the spectra of the porous SiC films. From this comparison the unique features seen in the porous SiC reflectance spectra can be interpreted.

[a)]Electronic mail: devaty@vms.cis.pitt.edu

II. EXPERIMENT

The porous layers were produced from single-crystal *p*-type 6H SiC wafers, approximately 300 μm thick. Aluminum contacts were deposited by evaporation on the Si face of the wafer, lead wires were attached, and then the samples were encapsulated in black wax so as to expose only the carbon face of the SiC wafer to the etch. The samples were placed into a Teflon cell with a platinum wire counter electrode and a saturated calomel reference electrode. Dilute aqueous HF served as the electrolyte. Anodization current densities ranging from 5 to 30 mA/cm^2 were used.

Room-temperature infrared reflectance spectra were measured at near normal incidence (5°) using a Fourier transform infrared (FTIR) spectrometer. The resolution was 1 cm^{-1}. A KBr beam splitter and a deuterated triglycine sulfate (DTGS) detector with a KBr window, range 400–5200 cm^{-1}, were used for the measurement. A 2000 Å-thick Pt film was used as a reflectance standard.

III. DATA

Figure 1 shows the room-temperature infrared reflectance near the reststrahl region for four thick, *p*-type, porous 6H SiC films. The porous SiC layers were prepared with current densities, porosities, and layer thicknesses as indicated in Fig. 1. Two of the samples [shown in Figs. 1(a) and 1(b)] were etched with the same current density and have the same porosity, although the porous layer thicknesses are quite different. The porosities and thicknesses of the porous layers were determined by using electron micrographs and profilometry, respectively. The reflectance spectra taken from the back of the samples, Fig. 2, appear to be bulk 6H SiC reflectance spectra. This indicates that the samples are not etched all the way through to the back surface.

The film whose spectrum is shown in Fig. 1(a) had a small surface area, which may account for the lower intensity
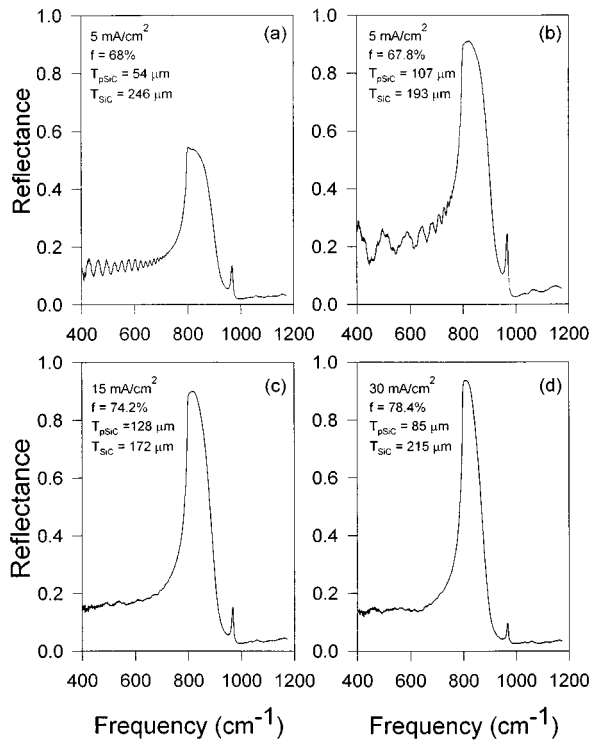
FIG. 1. Room-temperature reflectance (5°) of four porous p-type 6H SiC samples etched with various current densities. The porosities f, porous SiC layer thicknesses $T_{p\text{SiC}}$, and thicknesses of the residual SiC layers T_{SiC} are also listed in the figure.
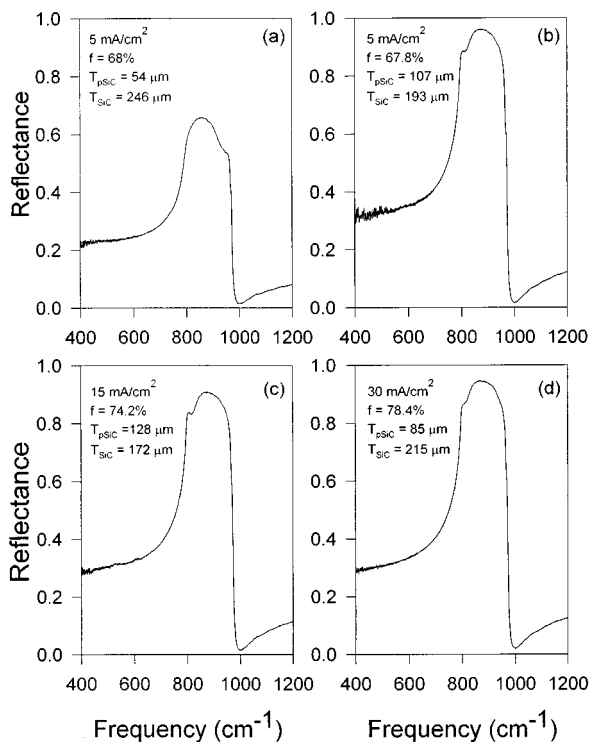

FIG. 2. Room-temperature back surface reflectance (5°) of four porous p-type 6H SiC samples etched with various current densities. The porosities f, porous SiC layer thicknesses $T_{p\text{SiC}}$, and thicknesses of the residual SiC layers T_{SiC} are also listed in the figure.
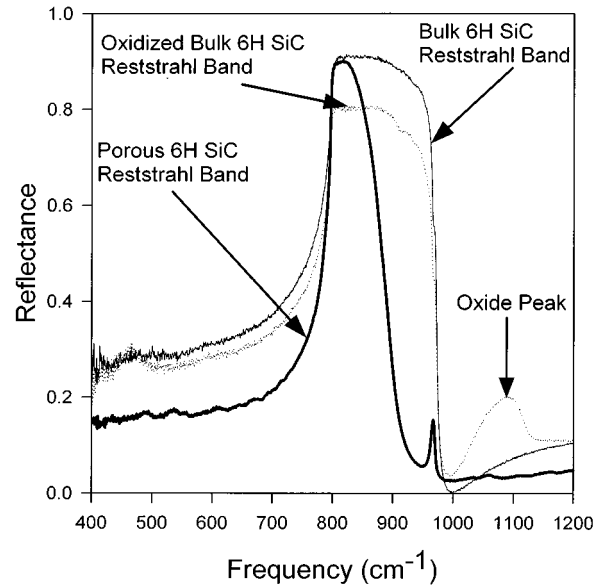

FIG. 3. Room-temperature reflectance (5°) of 128 μm-thick porous p-type 6H SiC layer on 172 μm 6H SiC (thick solid line) compared to bulk 6H SiC (thin solid line), and bulk 6H SiC with an 1100 Å SiO$_2$ layer (dotted line).

of its reflectance as compared to the other three samples shown. The porous SiC layer is approximately 69 μm thick as determined by matching fringes in the calculated spectrum to those seen in the data in the region 400–700 cm^{-1}. This optical estimate of the thickness is greater than the thickness determined by profilometry (54 μm), but this estimate is only as good as the estimate of the index of refraction of the porous material, which is based on a model described in Sec. IV. This optical estimate of the thickness implies that there is a bulk SiC layer ($\sim$231 μm thick) remaining below the porous layer, as observed from the back side reflectance of this sample [Fig. 2(a)].

The other porous SiC layer etched at 5 mA/cm^2 [Fig. 1(b)] also has interference fringes in the low-frequency region (below 700 cm^{-1}) but there are two overlapping sets of fringes in the reflectance of this sample making an optical determination of thickness difficult. The layers etched at 15 and 30 mA/cm^2 have no clear interference fringes from which to estimate thicknesses.

Figure 3 shows the room-temperature infrared reflectance near the reststrahl region for a thick, p-type, porous 6H SiC layer [same sample as Fig. 1(c)], compared with a bulk 6H SiC crystal, and a slightly oxidized bulk 6H SiC crystal. The p-type 6H SiC crystal from which the porous SiC layer was produced had a doping level of about 2×10^{18} cm^{-3}, and was approximately 300 μm thick before etching. The porous layer has a porosity of about 74.2% and a thickness of approximately 128 μm.

The oxide-free bulk 6H SiC shows a typical reststrahl region reflectance spectrum for 6H SiC. The rise in the reststrahl peak occurs near the SiC bulk transverse optical (TO) frequency, $\omega_{\text{TO}}=793.9$ cm^{-1}, and there is a sharp fall off in the reflectance near the bulk longitudinal optic (LO) frequency, $\omega_{\text{LO}}=970.1$ cm^{-1}. Details of the bulk reflectance of
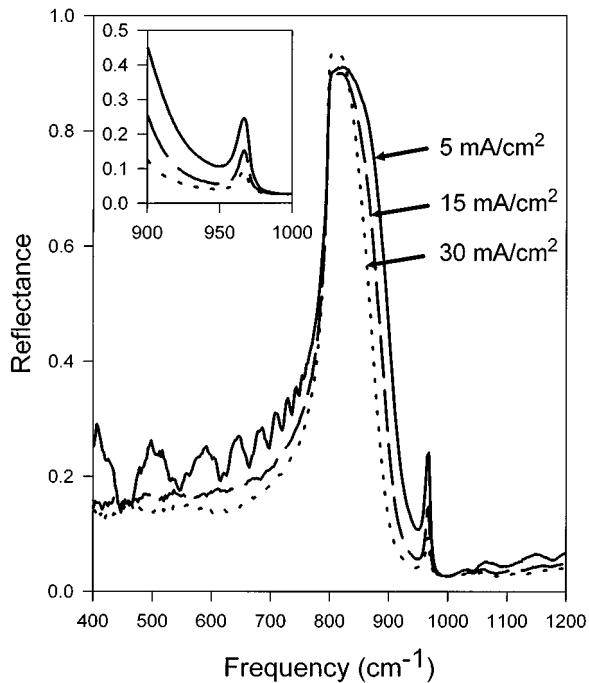
FIG. 4. Room-temperature reflectance (5°) of three *p*-type porous 6H SiC samples anodized at different current densities: (——) 5 mA/cm²; (-----) 15 mA/cm²; (.....) 30 mA/cm². The porosities of the samples are 67.8%, 74.2%, and 78.4%, and the porous SiC layer thicknesses are 107, 128, and 85 μm, respectively.

6H SiC and oscillator fits are discussed by Spitzer, Kleinman, and Walsh.[16]

The slightly oxidized bulk 6H SiC reflectance looks much the same as the oxide-free bulk reflectance except that there is an additional reflectance peak located near 1080 cm⁻¹. The oxide layer on this sample is approximately 1100 Å thick, as determined by matching fringes observed above 1200 cm⁻¹ (not shown) with the calculated spectrum. The 1080 cm⁻¹ peak is due to a SiO_2 layer that forms on the surface of the crystal when it is oxidized.[17] For extremely thin oxide layers the location of this peak shifts to lower frequency as the oxide thickness is decreased.[18] Samples with a SiO_2 layer as thin as a few hundred angstroms will show this peak in their reflectance spectra. This layer will form on both the carbon and silicon faces of the SiC crystal, but stronger reflectance signals are observed from oxides formed on the carbon face. This oxide layer is easily removed by dipping the SiC crystal in concentrated HF for 5 min, and samples thus treated display the bulk SiC reststrahl reflectance spectrum.

The reflectance spectrum of the porous SiC layer is very different from either of the SiC spectra discussed so far. Instead of a single broad reststrahl band, there are two bands in this region, one broad and one relatively sharp. Note that there is no evidence for the SiO_2 peak in the porous SiC spectrum indicating that the sample is not appreciably oxidized; however, there is a brownish tint to these samples which may be due to the presence of H_2SiF_6 stain from the electrochemical reaction.

Figure 4 shows the reflectance of three porous SiC layers prepared with current densities of 5, 15, and 30 mA/cm² and

having porosities of 67.8%, 74.2%, and 78.4% and layer thicknesses of 107, 128, and 85 μm, respectively. As can be seen in the figure, there is a definite shift to lower frequencies in the location of the high-frequency drop-off of the low-frequency reststrahl peak with increasing etch current density (increasing porosity). It may be possible to develop a calibration technique whereby the frequency of a specific feature in the reflectance spectrum (such as the high-frequency drop-off point in intensity of the low-frequency reststrahl peak) can be correlated to the porosity of the porous SiC layer. This would provide a simple, nondestructive technique for optically determining the porosity; however, further work is required to make a reliable calibration over the entire available porosity range (~35%–90%).
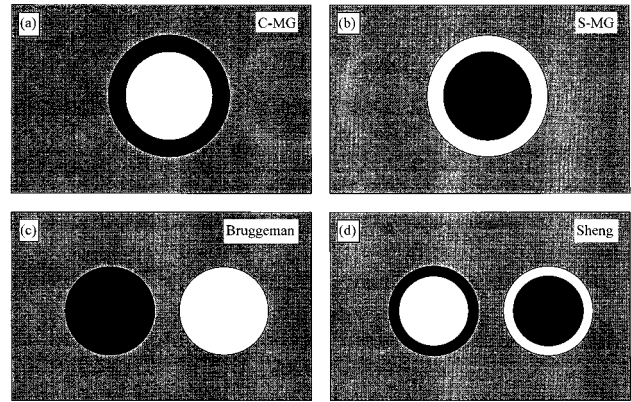

FIG. 5. Schematic of self-consistent imbedding of basic unit cells associated with the four effective medium models described in the text. The black regions represent 6H SiC, the white regions air, and the gray regions the homogeneous effective medium. The microscopic topologies are associated with the following models: (a) cavity-inclusion Maxwell–Garnett model (C-MG); (b) SiC-inclusion Maxwell–Garnett model (S-MG); (c) Bruggeman model; and (d) Sheng model.

IV. THEORY

To help interpret the new features seen in the infrared reflectance of porous 6H SiC, the data are compared to calculated spectra generated using the methods described by Piro.[19] Three effective medium theories, the Maxwell–Garnett model,[12] Bruggeman model,[13] and Sheng model,[14,15] were used to generate effective dielectric functions for the porous SiC layers for calculation of reflectance curves.

In order to model the dielectric tensor for a porous material, the microstructure of the material must be taken into account. Important parameters include the porosity and geometrical arrangement of the network of air cavities etched into the material. One way to approach this problem is to employ effective medium models which treat the dielectric function of a microscopically inhomogeneous material as a homogeneous dielectric function. This approach is based on the quasistatic approximation, i.e., it is only valid if the wavelength of the electromagnetic radiation is much greater than any of the particle, cavity, or cluster sizes within the material. There are many effective medium models,[11] and the choice of which one to employ depends on a number of factors, the most significant of which is the microstructural morphology of the material being modeled. Figure 5 shows

the assumed microstructural morphology of the four effective medium models that are used in this article.

Consider first the Maxwell–Garnett effective medium theory.[12] This model is based on the assumption that the underlying microstructure of the porous material can be reasonably described by coated spheres. For a two-component composite material, one material is called the host (or the coating material) and the other is called the inclusion (or the coated material). The treatment of the two materials is not symmetric. The topology of SiC coated air-filled spherical cavities is referred to as the cavity-inclusion Maxwell–Garnett (C-MG) model. The reverse topology, air-coated SiC spheres is referred to as the SiC-inclusion Maxwell–Garnett (S-MG) model.

The frequency-dependent, complex dielectric function $\bar{\epsilon}(\omega)$ generated by the C-MG model is given by[12]

$$\bar{\epsilon}(\omega) = \widetilde{\epsilon}_{\text{SiC}}(\omega)\epsilon'_{\infty}\left(\frac{\omega^2 - \omega_L'^2 + i\gamma\omega}{\omega^2 - \omega_T'^2 + i\gamma\omega}\right), \quad (1)$$

where

$$\widetilde{\epsilon}_{\text{SiC}}(\omega) = \epsilon_{\infty}\frac{\omega^2 - \omega_L^2 + i\gamma\omega}{\omega^2 - \omega_T^2 + i\gamma\omega}, \quad (2)$$

is the model bulk dielectric function for 6H SiC. The anisotropy and multiple oscillator modes in 6H SiC are neglected. The parameters for this Lorentz oscillator are $\epsilon_{\infty} = 6.52$, $\omega_T = 793.9$ cm^{-1}, $\omega_L = 970.1$ cm^{-1}, and $\gamma = 4.763$ cm^{-1}, as taken from Spitzer and co-workers[16] with ϵ_{∞} as modified by Patrick and Choyke.[20] The dielectric function used for air is $\epsilon_{\text{Air}}(\omega) = 1$. The primed parameters in Eq. (1) are given by

$$\epsilon'_{\infty} = \frac{(2f+1) + 2(1-f)\epsilon_{\infty}}{(1-f) + (f+2)\epsilon_{\infty}}, \quad (3)$$

$$\omega_L'^2 = \frac{(2f+1) + 2(1-f)\epsilon_0}{(2f+1) + 2(1-f)\epsilon_{\infty}}\omega_T^2, \quad (4)$$

and

$$\omega_T'^2 = \frac{(1-f) + (f+2)\epsilon_0}{(1-f) + (f+2)\epsilon_{\infty}}\omega_T^2, \quad (5)$$

where f is the porosity of the material.

For the S-MG model the frequency dependent complex dielectric function is

$$\bar{\epsilon}(\omega) = \epsilon'_{\infty}\left(\frac{\omega^2 - \omega_L'^2 + i\gamma\omega}{\omega^2 - \omega_T'^2 + i\gamma\omega}\right), \quad (6)$$

where

$$\epsilon'_{\infty} = \frac{(2f+1)\epsilon_{\infty} + 2(1-f)}{(1-f)\epsilon_{\infty} + (f+2)}, \quad (7)$$

$$\omega_L'^2 = \frac{(2f+1)\epsilon_0 + 2(1-f)}{(2f+1)\epsilon_{\infty} + 2(1-f)}\omega_T^2, \quad (8)$$

and

$$\omega_T'^2 = \frac{(1-f)\epsilon_0 + (f+2)}{(1-f)\epsilon_{\infty} + (f+2)}\omega_T^2. \quad (9)$$

Another effective medium theory commonly used to model composite systems is the Bruggeman model.[13] In this model the spherical inclusions of both air and SiC are imbedded in the effective medium. Unlike the Maxwell–Garnett models the component materials are treated symmetrically in this model. In order to obtain the effective dielectric function for this model the following quadratic equation must be solved:

$$\frac{f[\widetilde{\epsilon}_{\text{Air}}(\omega) - \bar{\epsilon}(\omega)]}{\widetilde{\epsilon}_{\text{Air}}(\omega) + 2\bar{\epsilon}(\omega)} + \frac{(1-f)[\widetilde{\epsilon}_{\text{SiC}}(\omega) - \bar{\epsilon}(\omega)]}{\widetilde{\epsilon}_{\text{SiC}}(\omega) + 2\bar{\epsilon}(\omega)} = 0. \quad (10)$$

There are two solutions to this equation but the correct solution for $\bar{\epsilon}(\omega)$ has a positive imaginary part, corresponding to dissipation.

Yet another effective medium theory used to model composite systems is the Sheng model.[14,15] In this model the spherical inclusions of air-coated SiC and SiC-coated air particles are imbedded in the effective medium. Like the Bruggeman model, the component materials are treated symmetrically in this model. In order to obtain the effective dielectric function for this model the following quadratic equation must be solved:

$$\frac{p[\widetilde{\epsilon}_1(\omega) - \bar{\epsilon}(\omega)]}{\widetilde{\epsilon}_1(\omega) + 2\bar{\epsilon}(\omega)} + \frac{(1-p)[\widetilde{\epsilon}_2(\omega) - \bar{\epsilon}(\omega)]}{\widetilde{\epsilon}_2(\omega) + 2\bar{\epsilon}(\omega)} = 0, \quad (11)$$

where p corresponds to the fraction of SiC-coated air cavities in the effective medium. The functions $\widetilde{\epsilon}_1$, $\widetilde{\epsilon}_2$, and the parameter p are given by

$$\widetilde{\epsilon}_1(\omega) = \frac{\widetilde{\epsilon}_{\text{SiC}}(\omega)\{2f[\widetilde{\epsilon}_{\text{Air}}(\omega) - \widetilde{\epsilon}_{\text{SiC}}(\omega)] + [2\widetilde{\epsilon}_{\text{SiC}}(\omega) + \widetilde{\epsilon}_{\text{Air}}(\omega)]\}}{\{[2\widetilde{\epsilon}_{\text{SiC}}(\omega) + \widetilde{\epsilon}_{\text{Air}}(\omega)] - f[\widetilde{\epsilon}_{\text{Air}}(\omega) - \widetilde{\epsilon}_{\text{SiC}}(\omega)]\}}, \quad (12)$$

$$\widetilde{\epsilon}_2(\omega) = \frac{\widetilde{\epsilon}_{\text{Air}}(\omega)\{2(1-f)[\widetilde{\epsilon}_{\text{SiC}}(\omega) - \widetilde{\epsilon}_{\text{Air}}(\omega)] + [2\widetilde{\epsilon}_{\text{Air}}(\omega) + \widetilde{\epsilon}_{\text{SiC}}(\omega)]\}}{\{[2\widetilde{\epsilon}_{\text{Air}}(\omega) + \widetilde{\epsilon}_{\text{SiC}}(\omega)] - (1-f)[\widetilde{\epsilon}_{\text{SiC}}(\omega) - \widetilde{\epsilon}_{\text{Air}}(\omega)]\}}, \quad (13)$$

and

$$p = \frac{(1 - f^{1/3})^3}{(1 - f^{1/3})^3 + (1 - (1-f)^{1/3})^3}. \quad (14)$$

The fraction of SiC-coated air cavities in the effective medium p is determined by a free volume argument. p is proportional to the number of possible configurations of an air sphere of radius r within a larger SiC sphere of radius R. Assuming that all configurations are equally probable, $p \sim (1 - r/R)^3$. Since $f = (r/R)^3$, Eq. (14) follows immedi-
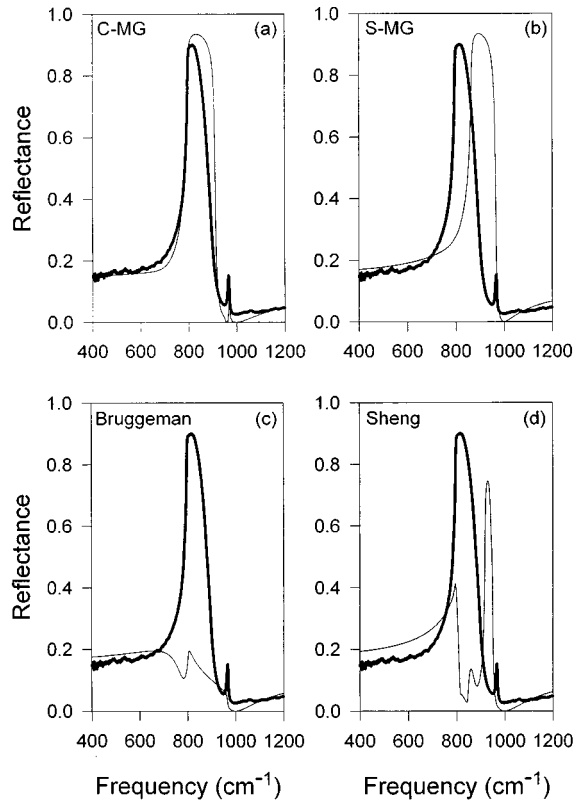
FIG. 6. Room-temperature reflectance (5°) of a 128 μm-thick porous SiC layer on a 172 μm 6H SiC layer and calculated reflectance spectra generated using effective medium models. Thick lines: data; thin lines: models.

FIG. 7. Expanded view of Fig. 6. Thick lines: data; thin lines: models.

ately. Again there are two solutions to Eq. (11) with the correct solution having a positive imaginary part of $\bar{\epsilon}(\omega)$, corresponding to dissipation.

V. COMPARISON OF POROUS SiC REFLECTANCE TO CALCULATED REFLECTANCE

The effective dielectric functions described in Sec. IV are used to calculate reflectance spectra based on the techniques described by Piro.[19] Since the FTIR instrument has a converging incident beam, the effect of the solid angle was estimated by calculating a rms average angle of incidence of 7.2° for 5° angle of incidence. The porous SiC layer was modeled as an isotropic medium and the residual SiC substrate was modeled as a uniaxial medium oriented with the c axis perpendicular to the interface between the two media. In this case, the reflectance can be broken up into independent components with electric-field vectors polarized either parallel (p) or perpendicular (s) to the plane of incidence. Both s and p polarizations are included, corresponding to unpolarized radiation. Interference effects in the porous SiC layers are neglected for samples showing no fringes in the reflectance spectrum, but they can be included for samples with fringes. Multiple reflections from within the substrate are neglected.

Figure 6 shows the measured spectrum from the 128-μm-thick, 74.2% porous SiC sample and the calculated spectra based on the C-MG, S-MG, Bruggeman, and Sheng models. In the calculated spectra the thicknesses of the porous
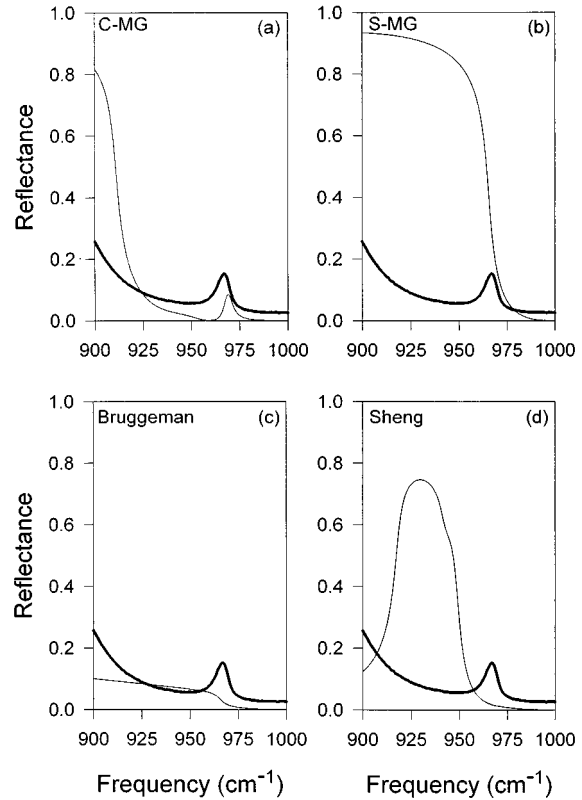
SiC layer and the residual bulk SiC layer are set to 128 and 172 μm, respectively. Interference effects are neglected in the porous layer since no fringes are observed in this spectrum. The levels of the calculated and measured reflectance spectra most closely match when multiple reflections are neglected in the residual bulk SiC layer. Figure 7 shows an expanded view of the region shown in Fig. 6.

The S-MG, Bruggeman, and Sheng models fail to reproduce the data, while the C-MG model replicates the main features of the measured spectrum. The failure of the S-MG model is expected since the microstructural topology described by this model, air-coated SiC particles, is physically unreasonable. The Bruggeman model is also inadequate for describing the porous system. Clearly, the only model that reproduces the main features of the measured spectrum is the C-MG model. The fact that the Sheng model fails to reproduce the measured spectrum may seem surprising since the Sheng model is in a sense a combination of the C-MG and S-MG models. However, the p parameter [Eq. (14)], which determines the relative fraction of SiC-coated air spheres in the effective medium, is extremely small ($p=0.017$) for the porosity of this sample ($f=0.742$). The air-coated SiC microstructure of the S-MG model dominates in this case. This accounts for the qualitative similarities between the Sheng and S-MG models, especially the large reflectance peak near 925 cm^{-1}.

VI. DISCUSSION

In order to understand the reststrahl region reflectance of porous SiC, consider first the reststrahl reflectance of bulk
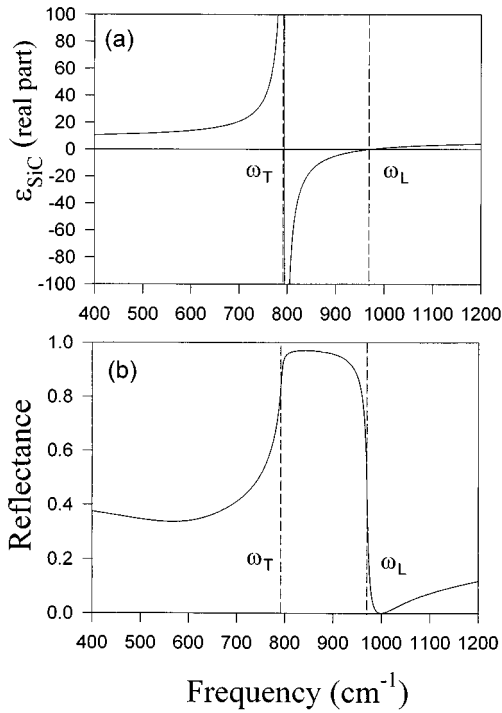
FIG. 8. (a) Calculated real part of the frequency-dependent dielectric function of bulk 6H SiC from Eq. (2) and (b) the corresponding reststrahl reflectance of bulk 6H SiC. The oscillator frequencies ω_T and ω_L are indicated on the graphs by dashed lines.
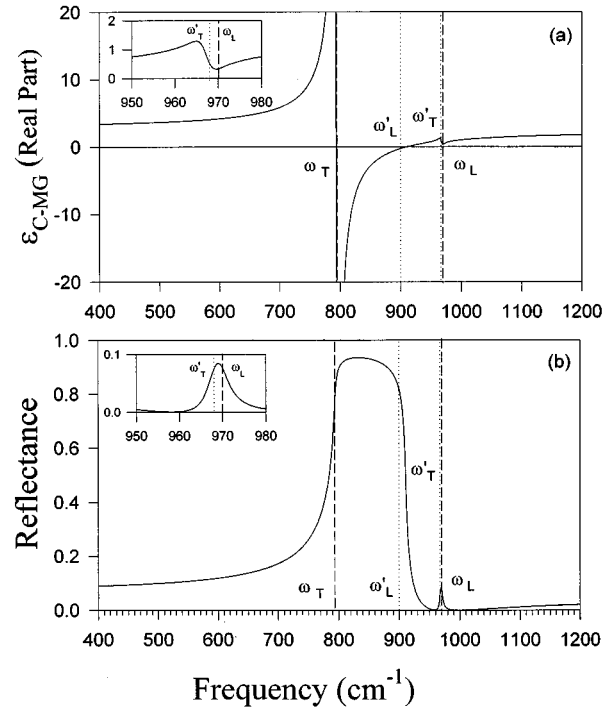
FIG. 9. (a) Calculated real part of the frequency-dependent dielectric function of p-type porous 6H SiC ($f=0.742$) from Eq. (1) and (b) the corresponding reflectance of p-type porous 6H SiC. The oscillator frequencies ω_T and ω_L are indicated on the graphs by dashed lines and the oscillator frequencies ω_T' and ω_L' are indicated by dotted lines.

6H SiC. Figure 8 shows the real part of the frequency-dependent dielectric function for bulk 6H SiC [Eq. (2)] in the reststrahl region of the spectrum along with the calculated reststrahl reflectance of a semi-infinite half-space of 6H SiC. The frequencies ω_T and ω_L are indicated on the graphs with vertical dashed lines. The frequency ω_T is the resonance frequency of the dielectric function and it corresponds to the onset of a region where $\epsilon(\omega)<0$ (neglecting damping).[21] This region is characterized by a high extinction coefficient (k) and high reflectance, as can be seen from Fig. 8. The frequency ω_L is defined as the frequency at which the real part of the dielectric function crosses zero (again neglecting damping). It also corresponds to the drop-off in the reflectance of the reststrahl band.

Figure 9 shows the real part of the frequency-dependent dielectric function for porous SiC ($f=0.742$) based on the C-MG model [Eq. (1)] in the reststrahl region along with the calculated reflectance of a semi-infinite half-space of porous SiC. The frequencies ω_T and ω_L are denoted on the graphs with dashed lines and the frequencies ω_T' and ω_L' are indicated with dotted lines. Referring to Fig. 9(a) we see that the dielectric function displays two-oscillator behavior covering the frequency regions ω_T to ω_L' and ω_T' to ω_L as compared to one-oscillator behavior for bulk 6H SiC (ω_T to ω_L). The corresponding reflectance of the porous SiC in this region shows two bands (ω_T to ω_L' and ω_T' to ω_L) as compared to one band seen in the bulk 6H SiC case (ω_T to ω_L). The peak reflectance of the second band (ω_T' to ω_L) is much less than that of the first (ω_T to ω_L').

Next consider a single spherical air cavity inside a piece of bulk 6H SiC. If an electric field is applied to the SiC then the relationship between the field inside the air cavity and the field in the SiC, assuming quasistatic boundary conditions, is[22]

$$\mathbf{E}_{\text{Air}}=\frac{3\,\epsilon_{\text{SiC}}(\omega)}{2\,\epsilon_{\text{SiC}}(\omega)+\epsilon_{\text{Air}}}\,\mathbf{E}_{\text{SiC}}. \qquad (15)$$

There is a resonance when the denominator of Eq. (15) goes to zero (neglecting damping),

$$2\,\epsilon_{\text{SiC}}(\omega)+\epsilon_{\text{Air}}=0. \qquad (16)$$

This leads to the resonance condition

$$\epsilon_{\text{SiC}}(\omega)=-\tfrac{1}{2}. \qquad (17)$$

The corresponding resonance frequency is

$$\omega^{*}=\omega_T\left(\frac{2\,\epsilon_0+1}{2\,\epsilon_{\infty}+1}\right)^{1/2}=959\ \text{cm}^{-1}. \qquad (18)$$

The differences in the reststrahl region reflectance seen in the porous SiC spectra, compared to bulk SiC, are associated with polarization effects introduced by the cavities combined with a mean-field average of interactions among the cavities. Physically, the situation can be described in the following way.[23] First, the reflectance starts to rise below the
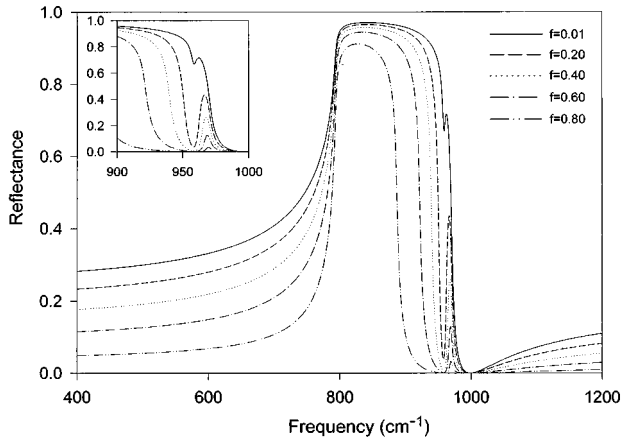
FIG. 10. Calculated normal incidence reflectance curves for an infinite half-space of porous SiC for several different porosities, indicated on the figure.

FIG. 11. Room-temperature reflectance (5°) of a 128 μm-thick porous 6H SiC layer on a 172 μm 6H SiC layer. Thick line: data; thin line: C-MG model.

bulk TO frequency (ω_T=793.7 cm^{-1}) and it stays high up to the frequency ω_L' [Eq. (4)]. For a f=0.742 porous SiC layer, $\omega_L' = 899.5$ cm^{-1}. At this frequency the external applied electric field polarizes the SiC surrounding an air cavity and induces a dipole field centered on the cavity. This causes the SiC around all other nearby cavities to polarize in such a way that their dipole fields drive the original polarization of the first cavity. In the absence of damping, a self-sustained collective longitudinal oscillation of the charges on the cavity surfaces will occur at the frequency ω_L'. The reflectance intensity will drop off at this frequency as it drops off at the bulk longitudinal oscillation frequency ω_L in bulk 6H SiC. There is another resonance due to the presence of the air cavities. The frequency of this resonance is shifted higher than the frequency of a single cavity resonance due to the interactions among the cavities. For a f=0.742 porous SiC layer, $\omega_T' = 968.0$ cm^{-1} [Eq. (5)]. The bulk SiC longitudinal oscillation at ω_L=970.1 cm^{-1} remains as well, and this is the frequency of the drop-off in reflectance of the second band.

Figure 10 shows the reflectance of an infinite half-space of porous SiC for several porosities ranging from f=0.01 to f=0.80 generated with the C-MG model. If there are only a very few cavities present in the medium the reflectance looks like the bulk 6H SiC reststrahl band with a sharp dip at 959 cm^{-1}. As the number of cavities is increased the dip gets deeper and broadens out so that there are two distinct bands in the reflectance spectrum. As the porosity is increased the frequency ω_L' [Eq. (4)] decreases, so the frequency at which the reflectance from the first band drops off is also lowered. As the porosity increases the frequency ω_T' [Eq. (5)] increases (very slowly), so the frequency at which the reflectance from the second band starts to rise also shifts toward higher frequencies.

We can now understand the reflectance of the porous SiC layer by referring to Fig. 11 which shows the reflectance of the 128 μm-thick, f=0.742 porous layer on 172 μm of residual 6H SiC along with the calculated spectrum from the C-MG model. The reflectance consists of two distinct bands as compared to one reststrahl band in bulk 6H SiC. A strong band covers the interval from the bulk TO frequency, ω_T=793.9 cm^{-1}, to $\omega_L' = 899.5$ cm^{-1}, the frequency associ-
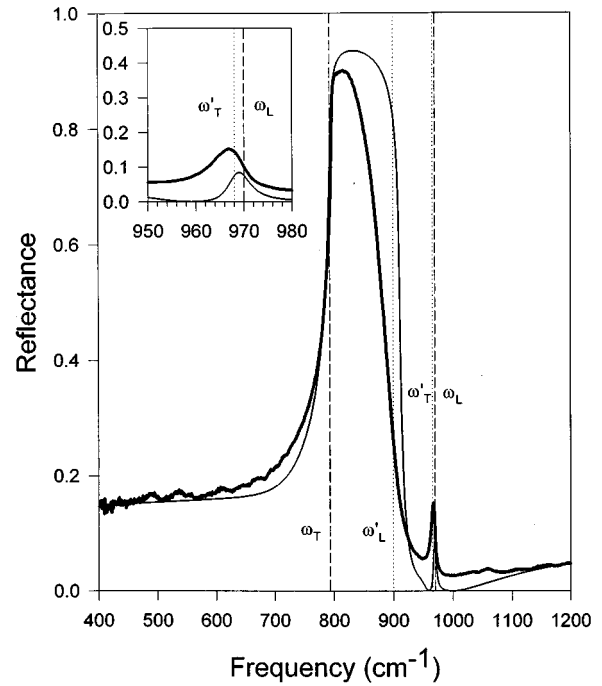
ated with the longitudinal oscillation of charges on the cavity surfaces. The second weak band rises near $\omega_T' = 968.0$ cm^{-1} (see inset Fig. 11) and falls off near the bulk LO frequency, ω_L=970.1 cm^{-1}.

VII. CONCLUSIONS

In conclusion, we have measured the room-temperature infrared reflectance of thick p-type porous 6H SiC layers at near-normal incidence. The reflectance spectrum of porous SiC is qualitatively different from that of bulk 6H SiC crystals, either oxidized or oxide free. The lack of an oxide peak in the porous SiC reflectance spectra indicates that the samples are not appreciably oxidized. Calculated reflectance spectra of one of the porous SiC layers were generated using four effective medium models. The best match to the data was obtained by using a Maxwell–Garnett model with the SiC acting as the host material and the air pockets acting as the inclusion material. This model fits the data quite well and reproduces the two bands observed in the measured spectra. There is a definite shift to lower frequencies in the location of the high-frequency drop-off in intensity of the low-frequency band with increasing anodization current density and, hence, porosity. Infrared reflectance may provide a diagnostic technique whereby the porosity of the layers can be determined by the location of a feature in the reflectance spectrum; however, further work is required to achieve this calibration.

ACKNOWLEDGMENTS

Mac Millan *et al.*

[1] L. T. Canham, Appl. Phys. Lett. **57**, 1046 (1990).

[2] I. A. Belogorokhov, V. A. Karavanskiĭ, A. N. Obraztsov, and V. Yu. Timoshenko, JETP Lett. **60**, 274 (1994).

[3] S. Hongtao *et al.*, in Proceedings of the 21st International Conference on the Physics of Semiconductors, Beijing, China, 1992, Vol. 2, p. 1459.

[4] J. S. Shor, I. Grimberg, B. Z. Weiss, and A. D. Kurtz, Appl. Phys. Lett. **62**, 2836 (1993).

[5] H. Mimura, T. Matsumoto, and Y. Kanemitsu, Appl. Phys. Lett. **65**, 3350 (1994).

[6] T. Matsumoto, J. Takahashi, T. Tamaki, T. Fugati, H. Mimura, and Y. Kanemitsu, Appl. Phys. Lett. **64**, 226 (1994).

[7] A. M. Danishevskiĭ, V. B. Shuman, A. Yu. Rogachev, and P. A. Ivanov, Semicond. **29**, 1106 (1995) [Fiz. Tekh. Poluprovodn. **29**, 2122 (1995)].

[8] J. S. Shor, L. Bemis, A. D. Kurtz, I. Grimberg, B. Z. Weiss, M. F. Mac-Millan, and W. J. Choyke, J. Appl. Phys. **76**, 4045 (1994).

[9] J. S. Shor, L. Bemis, A. D. Kurtz, M. F. Mac Millan, W. J. Choyke, I. Grimberg, and B. Z. Weiss, Inst. Phys. Conf. Ser. **137**, 193 (1993).

[10] A. O. Konstantinov, C. I. Harris, and E. Janzén, Appl. Phys. Lett. **65**, 2699 (1994).

[11] M. F. MacMillan, R. P. Devaty, and J. V. Mantese, Phys. Rev. B **43**, 13 838 (1991).

[12] J. C. M. Garnett, Philos. Trans. R. Soc. London Ser. A **203**, 385 (1904); **205**, 237 (1906).

[13] D. A. G. Bruggeman, Ann. Phys. (Leipzig) **24**, 636 (1935).

[14] P. Sheng, Phys. Rev. Lett. **45**, 60 (1980).

[15] U. J. Gibson, H. G. Craighead, and R. A. Buhrman, Phys. Rev. B **25**, 1449 (1982).

[16] W. G. Spitzer, D. A. Kleinman, and D. Walsh, Phys. Rev. **113**, 127 (1959).

[17] C. Martinet and R. A. B. Devine, J. Appl. Phys. **77**, 4343 (1995).

[18] W. G. Spitzer and D. A. Kleinman, Phys. Rev. **121**, 1324 (1961).

[19] O. E. Piro, Phys. Rev. B **36**, 3427 (1987).

[20] L. Patrick and W. J. Choyke, Phys. Rev. B **2**, 2255 (1970).

[21] F. Wooten, *Optical Properties of Solids* (Academic, New York, 1972), Chap. 3.

[22] J. D. Jackson, *Classical Electrodynamics*, 2nd corrected ed., John (Wiley, New York, 1975), p. 151.

[23] A. S. Barker, Jr., Phys. Rev. B **7**, 2507 (1973).